

A Novel Fuzzy Non-Homogeneity Measure Based Kernelized Image Segmentation For Noisy Images

Satrajit Mukherjee, Bodhisattwa Prasad
Majumder

Dept. of ETCE, Jadavpur University
Kolkata 700 032, India.

satra0293@gmail.com, mbodhisattwa@gmail.com

Aritran Piplai
Dept. of CSE, Jadavpur
University

Kolkata 700 032, India.

aritraniplai@gmail.com

Swagatam Das
Electronics and Communication
Sciences Unit, Indian Statistical
Institute

Kolkata – 700 108, India.

swagatam.das@ieee.org

Abstract— The paper proposes a novel non-homogeneity measure based kernelized image segmentation algorithm for noisy images. Every 3×3 neighbourhood of every single pixel is considered for generating localized spatial domain non-homogeneity measures for every individual window. Then these spatial domain non-homogeneity measures are converted into fuzzy domain non-homogeneity coefficients by aggregating the localized measures into a single distribution and then deriving fuzzy domain values from a Gaussian membership function. Quantitative analyses have been rendered with respect to state-of-the-art noisy-image segmentation techniques and results show improved performance. Speckle-noise ridden SAR images and Rician noise ridden medical images are finally considered to show real-life applications of our algorithm.

Keywords- Fuzzy membership, non-homogeneity, kernel, Speckle noise, Rician noise, SAR, MRI, segmentation accuracy.

I. INTRODUCTION

Image segmentation constitutes an important part of image processing which has various applications in the fields of feature extraction and object recognition. Segmentation methods mainly involve clustering techniques [1]-[5] which separate a set of data points, or vectors, into different non-overlapping groups, such that the members of a particular group or cluster are similar to each other. Recent researches have led to the development of fuzzy segmentation methods which associate fuzzy membership values to each image pixel for its tendency to belong to various clusters. Fuzzy c-means clustering [6][7], when applied to image segmentation, partitions an image into c pre-specified number of clusters and associates fuzzy values for each individual image pixel to belong to a particular cluster. However, the conventional fuzzy c-means algorithm is not immune to noise and does not take into account the spatial information associated with every individual pixel.

Szilagyi *et. al* [8] proposed an enhancement of the conventional FCM clustering method (EnFCM) based on the histogram of a linearly-weighted summed image obtained from the aggregate information of the local neighbourhood of each pixel and original image. Cai *et. al* [9] introduced a spatial similarity measure to generate a non-linearly weighted summed image. This fast generalized (FGFCM) algorithm includes both gray-level and spatial information. But these methods are dependent on several heuristics and parameters which vary according to the complexities of images. Hence the optimal choice of these parameters is very difficult, thus making these methods non-robust, especially for noisy images.

To do away with the problem of excessive parameterization, Stelios *et. al* [10] proposed a parameter-free fuzzy local information c-means clustering (FLICM) scheme. Gong *et. al* have extended their work to a new variant of FLICM, which is RFLICM [11] but the drawback of this algorithm is that it fails to take spatial constraints into account.

Most of the clustering algorithms in previous literature including the abovementioned schemes use Euclidean norm, which is non-robust as in the case of non-Euclidean input data set. Kernel based methods [12]-[15] of segmentation transform data points; in this case, image features into a higher dimensional space which makes segmentation easy. It is basically a method in which the lower dimension inner product space is transformed into a higher dimensional space using non-linear mapping.

The existing kernel based image segmentation methods work sufficiently well in case of noisy images but the method proposed by Chen *et. al* [16] uses the mean of the surrounding pixels of a particular image pixel in the objective function as a measure of the spatial information. This creates a problem because it puts equal weights on all of the surrounding pixels of a particular pixel during computation. More importantly, this method does not take into account the pixel intensity deviations in a particular window around a pixel of concern.

Gong *et. al* [17] recently proposed a kernel based fuzzy clustering scheme that takes into account spatial constraints and neighbourhood information. But the trade-off weighted fuzzy factor which changes the contribution of neighbourhood pixels, as proposed by the authors, is only dependant on local coefficients of variation and independent noise distributions in localized windows. Our proposed method incorporates spatial constraints and local information by calculating the weighted mean of the surrounding pixels, the weights being reciprocal to the Cartesian distances between the coordinates of the centre pixel and that of the surrounding pixels. However, the foundation of our algorithm lies in extracting the ‘non-homogeneity’ information from all localized windows and forming a composite distribution over the entire image. Fuzzy non-homogeneity coefficients are then derived by transforming the spatial domain localized ‘non-homogeneity’ values into fuzzy domain values by utilizing the standard deviation of the composite distribution. In the point of noise immunity, our method serves more robustness than the other competing algorithms as shown by experimental results for different kinds of noise such as Salt and Pepper, Speckle, Gaussian, Poisson and Rician noise. A speckle noise ridden Synthetic Aperture Radar (SAR) [18]-[19] images and a Rician [20]-[21] noise ridden medical image are considered for testing.

The organization of the paper is as follows:-

Section II provides the framework of the original kernel based work proposed by Chen *et. al.* Section III introduces the weighted neighbourhood information while sections IV and V introduce the spatial domain and fuzzy domain non-homogeneity measures respectively. Section VI proposes the modified kernel based objective function while Section VII provides experimental results. Applications to SAR and Medical Images and computational complexities are found in Sections VIII and IX while section X concludes the proceedings.

II. FRAMEWORK OF THE ORIGINAL KERNEL BASED IMAGE SEGMENTATION

Chen *et. al* proposed a variant of FCM [16] which takes into account the spatial constraints of each individual pixel.

$$J_m = \sum_{i=1}^c \sum_{k=1}^N u_{ik}^m \|x_k - v_i\|^2 + \frac{\alpha}{N_R} \sum_{i=1}^c \sum_{k=1}^N u_{ik}^m \sum_{r \in N_k} \|x_r - v_i\|^2 \quad (1)$$

Eq. (1) gives the objective function that needs to be minimized to form the desired clusters. The second term in this objective function is the metric for the spatial information which is necessary to overcome the shortcomings of classical FCM. It tries to maintain homogeneity with the neighbouring pixels. But this method is computationally complex. In each iteration, the pixels in a window of size k need to be taken into account.

To tackle this problem, a simple mathematical modification was made. The term $\frac{1}{N_R} \sum_{r \in N_k} \|x_r - v_i\|^2$ can be computed as $\frac{1}{N_R} \sum_{r \in N_k} \|x_r - \bar{x}_k\|^2 + \|\bar{x}_k - v_i\|^2$, where \bar{x}_k is the mean of the surrounding pixels. This makes the objective function computationally less expensive as \bar{x}_k can be computed in advance.

Thus the objective function based on spatial constraints reduced to the form in Eq. (2):

$$J_m = \sum_{i=1}^c \sum_{k=1}^N u_{ik}^m \|x_k - v_i\|^2 + \alpha \sum_{i=1}^c \sum_{k=1}^N u_{ik}^m \|\bar{x}_k - v_i\|^2 \quad (2)$$

The parameter α when set to zero, the objective function becomes a simple FCM objective function. If α is made infinite, minimization of the objective function yields the same result as classical FCM would on the median or mean filtered image.

Chen *et. al* used this particular method and kernel-induced distances to better the previous clustering scheme. $\Phi: \mathbf{x} \in X \subseteq R^d \rightarrow \Phi(\mathbf{x}) \in F \subseteq R^H (d \ll H)$ is a non-linear mapping which transforms a vector to another in a higher dimension as seen in Eq.(3).

If $\mathbf{x} = [x_1, x_2]^T$ and $\Phi(\mathbf{x}) = [x_1^2, \sqrt{2}x_1x_2, x_2^2]^T$ then the inner product can be defined as:

$$\Phi(\mathbf{x})^T \Phi(\mathbf{y}) = [x_1^2, \sqrt{2}x_1x_2, x_2^2]^T [y_1^2, \sqrt{2}y_1y_2, y_2^2] = (\mathbf{x}^T \mathbf{y})^2 = K(\mathbf{x}, \mathbf{y}) \quad (3)$$

An improvement of inner product calculation was to use the kernel function $K(\mathbf{x}, \mathbf{y})$ because using the transformation matrix was not necessary. A typical polynomial kernel is shown as:

$$K(\mathbf{x}, \mathbf{y}) = \exp\left(\frac{-\left(\sum_{i=1}^d |x_i - y_i|^a\right)^b}{\sigma^2}\right) \quad (4)$$

where d is the dimension of the vector and $a > 0; 1 \leq b \leq 2$;

$K(x, x) = 1$ for all x . A polynomial kernel of degree p can be formulated as:

$$K(\mathbf{x}, \mathbf{y}) = (\mathbf{x}^T \mathbf{y} + 1)^p \quad (5)$$

The kernel functions can be used instead of the inner products to construct the kernel space.

The clustering was performed by taking the centroids in the original space instead of taking them in a higher dimension such that interpretation of results would be easier. Using the mathematical formulations mentioned before the objective function was constructed as:

$$J_m = \sum_{i=1}^c \sum_{k=1}^N u_{ik}^m \|\Phi(\mathbf{x}_k) - \Phi(\mathbf{v}_i)\|^2 \quad (6)$$

Kernelized substitutions yielded Eq. (7).

$$\begin{aligned} \|\Phi(\mathbf{x}_k) - \Phi(\mathbf{v}_i)\|^2 &= (\Phi(\mathbf{x}_k) - \Phi(\mathbf{v}_i))^T (\Phi(\mathbf{x}_k) - \Phi(\mathbf{v}_i)) \\ &= \Phi(\mathbf{x}_k)^T \Phi(\mathbf{x}_k) - \Phi(\mathbf{x}_k)^T \Phi(\mathbf{v}_i) - \Phi(\mathbf{v}_i)^T \Phi(\mathbf{x}_k) + \Phi(\mathbf{v}_i)^T \Phi(\mathbf{v}_i) \\ &= K(\mathbf{x}_k, \mathbf{x}_k) + K(\mathbf{v}_i, \mathbf{v}_i) \\ &\quad - 2K(\mathbf{x}_k, \mathbf{v}_i) \end{aligned} \quad (7)$$

The original kernel based objective function proposed by Chen *et. al* is as follows:

$$J^{S\Phi} = \sum_{i=1}^c \sum_{k=1}^N (u_{ik}^m (1 - K(x_k, v_i))) + \alpha \sum_{i=1}^c \sum_{k=1}^N u_{ik}^m (1 - K(\bar{x}_k, v_i)) \quad (8)$$

The partition matrix values and centroids were presented as in Eqs. (9) and 10 respectively.

$$u_{ik} = \frac{\left(\left(1 - K(x_k, v_i)\right) - \alpha \left(1 - K(\bar{x}_k, v_i)\right)\right)^{\frac{1}{m-1}}}{\sum_{j=1}^c \left(\left(1 - K(x_k, v_j)\right) - \alpha \left(1 - K(\bar{x}_k, v_j)\right)\right)^{\frac{1}{m-1}}} \quad (9)$$

$$v_i = \frac{\sum_{k=1}^N u_{ik}^m (K(x_k, v_i) x_k + \alpha K(\bar{x}_k, v_i) \bar{x}_k)}{\sum_{k=1}^N u_{ik}^m (K(x_k, v_i) + \alpha K(\bar{x}_k, v_i))} \quad (10)$$

This method however does not take into account any spatial constraint and does not vary the contribution of either the nucleus or the neighbouring pixels. Thus, we propose a modification of the objective function in the next few sections.

III. WEIGHTED NEIGHBOURHOOD INFORMATION

0.707	1	0.707
1	0	1
0.707	1	0.707

Fig.1: 3×3 window showing the weights of contribution of the neighbours

The information from each neighbourhood pixel is made dependent on the Cartesian distance of a neighbour from the nucleus. Fig. 1 shows the weights of contribution of the neighbours, which are actually the inverse of their respective Cartesian distances from the center pixel. The weighted mean of these contributions will be used in place of the arithmetic mean as an initial modification of the Eq. proposed by Chen *et. al.*

The weighted neighbourhood information would be used to replace the arithmetic mean \bar{x}_k with the Cartesian-distance induced weighted mean \bar{x}_{wk} which is computed as shown in Eq. (11):

$$\bar{x}_{wk} = \frac{\sum_{i=1}^{N_r} \left(\frac{1}{d_i}\right) * I_i}{\sum_{i=1}^{N_r} \frac{1}{d_i}} \quad (11)$$

where I_i is the pixel intensity of a neighbouring pixel $i \in N_r$ and d_i is the Cartesian distance of the i -th neighbour from the centre pixel or the neighbour. Thus an initial modification of the kernel-based objective function can be given as:

$$JS^\Phi = \sum_{i=1}^c \sum_{k=1}^N (u_{ik}^m (1 - K(x_k, v_i)) + \alpha \sum_{i=1}^c \sum_{k=1}^N u_{ik}^m (1 - K(\bar{x}_{wk}, v_i))) \quad (12)$$

Here, we have not changed the contribution of the neighbouring pixels except for directly incorporating spatial constraints in the non-linear kernel mapping. The Cartesian distances of the neighbours from the nucleus have only been used to modify the inputs to the kernel mapping function and have not been used explicitly as damping coefficients. The next subsections introduce suppressing coefficients which would be used to further modify the kernel based function.

IV. AN INITIAL SPATIAL DOMAIN NON-HOMOGENEITY MEASURE

The deviations of the gray levels of the neighbouring 8 pixels with respect to the intensity of the centre pixel or the 'nucleus' are computed using Eq.(13) and the corresponding curve is given by Fig 2.

$$\delta(r, r_0) = \exp \left[- \left(\frac{I(r) - I(r_0)}{t} \right)^2 \right], \quad (13)$$

where ' r ' is the position of any neighbouring pixel, ' r_0 ' is the position of the nucleus, $I(r)$ is the intensity of any pixel, $I(r_0)$ is the intensity of the nucleus and ' t ' is a control parameter that controls the range of the output of the equation. The squared exponentially decaying function is taken to associate the same value of deviation for pixel intensities that are greater or smaller than the nucleus intensity by the same amount.

The outputs for the neighbouring 8 pixels from Eq. (13) are summed up to obtain an initial metric for quantizing the 'homogeneity information' or the net pixel intensity deviation in the window of concern. Eq. (14) represents the sum.

$$D(r, r_0) = \sum_r \delta(r, r_0) \quad (14)$$

As is evident from the equation, if a neighbouring pixel has the same intensity as the nucleus, the output would be 1. A perfectly homogeneous region would have all the neighbourhood pixel intensities equal to the nucleus intensity. In that case, the sum of the outputs for all of the 8 neighbouring pixels would be 8, with each output being equal to 1. This is the maximum value of the summed output. The choice of the parameter t depends on the minimum value of the output of Eq. (13). The maximum intensity deviation $I(r) - I(r_0)$ can be 255 for a grayscale image and we will limit the minimum value of the Eq. (13) to $1/8$ such that the minimum value of the summed output of Eq. (14) reduces to 1. Thus the value of the parameter t can be obtained by solving the equation in Eq. (15).

$$\exp \left[\left(\frac{(-255)}{t} \right)^2 \right] = 1/8 \quad (15)$$

This yields the value of the parameter t as 176.8344 such that the summed up output range of Eq. (14) lies within (1, 8).

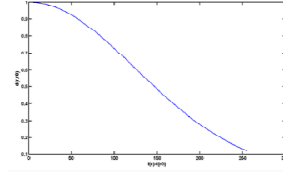


Fig 2: The deviation function δ plotted against intensity deviation $(I(r) - I(r_0))$

The inverse of this range i.e. $[1/8, 1]$ can be considered as an initial metric for the 'non-homogeneity information' in the window and we shall call this variable $k = \frac{1}{D}$, where we obtained the values of D using Eq. (14). However, the range of this metric is small and we shall modify it to arrive at a concrete expression for suppressing or enhancing the contribution of the nucleus subsequently.

V. FUZZY NON-HOMOGENEITY MEASURE

The entire kernel based objective function can be thought of as a summation of the contribution from the nucleus and the contribution of its neighbourhood. In case of a perfectly homogeneous region, the contributions of the neighbouring pixels have to be taken into account and thus the contribution of the nucleus needs to be suppressed. With increase in non-homogeneity, the contribution of the nucleus in the objective function is increased.

The initial non-homogeneity information proposed in section IV was in the range $[1/8, 1]$ and it is mapped to the fuzzy domain values $[0, 1]$ using the Eq. (16) which represents a Gaussian membership [22]-[24].

$$s(k) = \exp \left(- \left(\frac{(k_{max} - k)^2}{2 * \sigma_k^2} \right) \right), \quad (16)$$

where σ_k is the standard deviation of the values of all the spatial domain 'non-homogeneity' measure values obtained for all the localized windows i.e. k and k_{max} is the maximum value of the measure globally obtained in an image. Thus computation of σ requires that the values of k for all the localized windows be recorded such that their standard deviation can be evaluated. The maximum value of k can be '1' and the minimum value '1/8' as mentioned in section IV but it is dependent on the test image at hand.

The fuzzy mapping of the spatial domain non-homogeneity values increases the dynamic range of variation of the suppressing coefficients and associates fuzzy domain values in the range of $[0, 1]$.

VI. MODIFICATION OF OBJECTIVE FUNCTION

Thus the final modified function incorporates both spatial constraints by using the Cartesian induced weighted pixel intensities as input to the Kernel map as well as non-homogeneity information by using the fuzzified suppressing coefficients $s(k)$ which increase the contribution of the nucleus with increasing non-homogeneity. The modified kernel based equation can be presented in Eq. (17) as:

$$JS^\Phi = \sum_{i=1}^c \sum_{k=1}^N (s(k) * u_{ik}^m (1 - K(x_k, v_i)) + \alpha \sum_{i=1}^c \sum_{k=1}^N u_{ik}^m (1 - K(\bar{x}_{wk}, v_i))) \quad (17)$$

where $s(k)$ is given in Eq. (16).

Similarly, the partition matrix values u_{ik} and the centroids v_i are modified in Eqs. (18) and (19) respectively by incorporating the weighted mean and the suppressing coefficients. The values of m , α and σ of the kernel in Eq. (4) has been taken as 2, 3.8 and 150 respectively as proposed by Chen *et. alas* the variations of these parameters are not of important concern to our work.

$$u_{ik} = \frac{(s(k) * (1 - K(x_k, v_i)) - \alpha(1 - K(\bar{x}_{wk}, v_i)))^{-\frac{1}{m-1}}}{\sum_{j=1}^c (s(k) * (1 - K(x_k, v_j)) - \alpha(1 - K(\bar{x}_{wk}, v_j)))^{-\frac{1}{m-1}}} \quad (18)$$

$$v_i = \frac{\sum_{k=1}^n u_{ik}^m (s(k) * K(x_k, v_i) x_k + \alpha K(\bar{x}_{wk}, v_i) \bar{x}_k)}{\sum_{k=1}^n u_{ik}^m (s(k) * K(x_k, v_i) + \alpha K(\bar{x}_{wk}, v_i))} \quad (19)$$

The entire pseudocode of the algorithm is presented here. The optimization of the objective function is simply done using successive iteration method which is present in the pseudocode, showing necessary termination criterion for the optimization.

PseudoCode of our algorithm

Step 1 Define the number of desired clusters c and choose prototype centroids of these clusters and set $\epsilon=0.001$.
Step 2 Compute fuzzy non-homogeneity coefficients to set up mathematical expressions for the modified objective function, partition matrix values and centroids.

Step 3 Update the partition matrix values using Eq (17)

Step 4 Update the centroids using Eq (18)

Repeat Steps 3)-4) until the following termination criterion is satisfied:

$$\|V_{\text{new}} - V_{\text{old}}\| < \epsilon$$

where V has been defined previously and ϵ has been introduced in step 1.

VII. EXPERIMENTAL RESULTS

All the test images except for the image of the Cameraman have been taken from the Berkeley Segmentation Dataset (BSDS). (<http://www.eecs.berkeley.edu/Research/Projects/CS/vision/bsds>) The test images taken from BSDS are of size 481x321 while the image of the Cameraman is of size 256x256.

A. Qualitative Analysis

Qualitative Analysis has been shown with the help of three test images and with respect to the segmented images of the competing algorithms. The competing algorithms include a *Nystrom* method based spectral graph grouping algorithm NNCut [25], FLICM [10], RFLICM [11], WFLICM [17] and KWFLICM [17]. Figs. 4(a), 5(a) and 6(a) show a Salt and Pepper noise added Cameraman image, Gaussian noise added Zebra image and Poisson noise added Mushroom image. Poisson noise is generated from the image data instead of being artificially added.

Figs. 4(b), 5(b) and 6(b) show that the NNCut algorithm manages to preserve the structure of the image but fails to remove noises as can be seen from the noisy pixels left in these images. The FLICM and RFLICM algorithms only selectively remove noise and also suffer from blurry edges and distorted image structure as can be seen in Figs. 4(c)-(d), 5(c)-(d) and 6(c)-(d). The WFLICM and KFLICM perform particularly well in case of salt and pepper noise as they work mainly on localized windows but need improvement for distributed noise such as Gaussian and Poisson as can be seen from Figs. 5(e)-(f) and 6(e)-(f). Our proposed algorithm not only removes all types of noise but also preserves the shape of the image and the structure of the edges in the image as can be seen from Figs. 4(g), 5(g) and 6(g). It is to be noted that 3-level segmentation has been done for all the test cases.

The original images without noise are in Fig. 3.

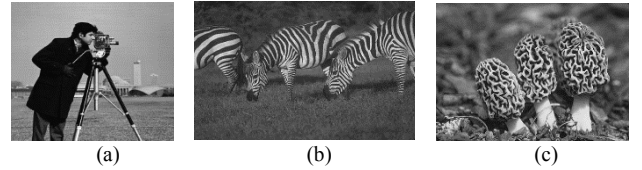


Fig. 3: a) Cameraman b) Zebra c) Mushroom Images

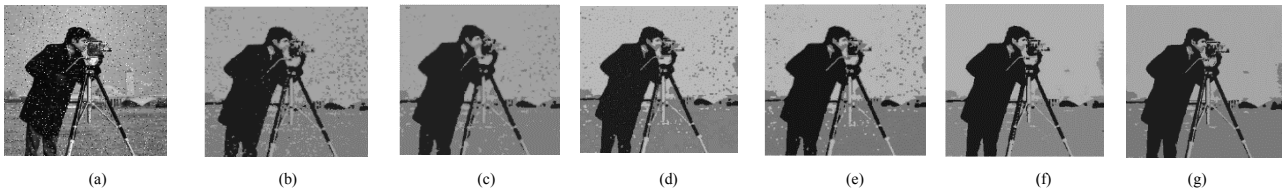


Fig. 4: a) Salt & pepper noise (30%) added Cameraman b) NNCUT c) FLICM d) RFLICM e) WFLICM f) KWFLICM g) Proposed method

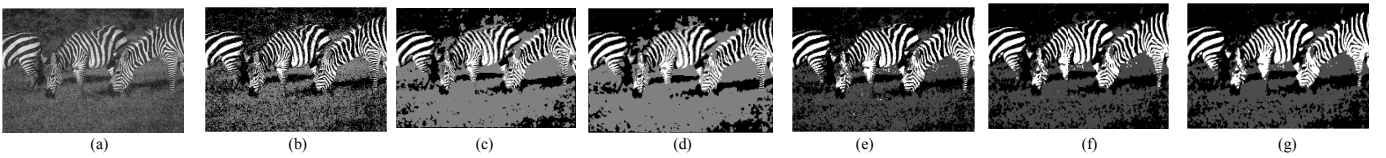


Fig. 5: a) Gaussian noise (30%) added Zebra b) NNCUT c) FLICM d) RFLICM e) WFLICM f) KWFLICM g) Proposed method

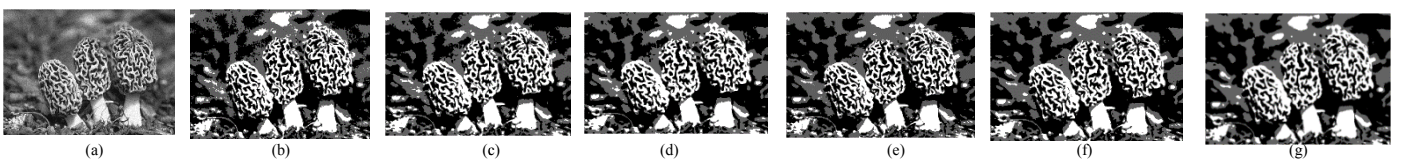


Fig. 6: a) Poisson noise added Mushroom b) NNCUT c) FLICM d) RFLICM e) WFLICM f) KWFLICM g) Proposed method

B. Quantitative Measures

Quantitative Analysis has been performed and tabulated on the basis of the metrics discussed in this section. The amount of Salt & Pepper and Gaussian noise was kept at both 20% and 30% while the Poisson noise, as previously mentioned, is generated from the image data itself. The results were averaged after 25 independent runs for all the test images and for all competing algorithms.

1) Measure dependant on ground truth

Segmentation Accuracy [26] is a metric used to measure the de-noising capabilities of different algorithms. It gives us an idea about the fraction of correctly assigned pixels. It is defined as the sum of the pixels which are correctly assigned divided by the sum of the total number of pixels and Eq. (20) shows the mathematical form of SA.

$$SA = \frac{\sum_{i=1}^c A_i \cap R_i}{\sum_{j=1}^c R_j} \quad (20)$$

Here c is the number of clusters A_i is the set of pixels which forms the i -th cluster in the algorithm and R_i represents the referenced image's set of pixels which constitute its i -th cluster. Here, the reference or ground truth images are obtained by segmenting the images without adding any noise to them using the conventional FCM algorithm and then using these ground truths to calculate the segmentation accuracy of all the competing algorithm for the noisy versions of the images.

Table I shows maximum segmentation accuracy with respect to all test images for all types of noise and for all competing algorithms. Higher is the value of SA, the more adequate is the clustering of pixels. By cluster adequateness, we mean that despite the presence of noise, the pixels of the noisy image would be assigned to those clusters which would have been assigned to the pixels had there been no noise in the image. Thus, the maximum value of SA achieved by our algorithm indicates that despite the presence of noise in the images to be segmented, the noise has been adequately removed and the pixels have been assigned to proper clusters. The NNCut algorithm achieves lowest value of SA because it fails to adequately remove noise, as a result of which many pixels have been abruptly assigned to different clusters. A qualitative look at Figs 4(b), 5(b) and 6(b) validate this claim as can be seen from the speckles in the images that have been assigned to different clusters with respect to their immediate background. Similarly, the lower values of SA for the other algorithms can be attributed to their inadequate removal of noise in comparison to our algorithm. In addition, the FLICM and RFLICM algorithms produce blurry edges which indicate that the edge or contour pixels have been assigned to improper clusters, a problem which is eradicated completely by our algorithm.

2) Measure independent of ground truth

In the absence of any ground truth, calculation of Segmentation Accuracy is impossible. An entropy-based objective function [27] was developed, minimization of which would maximize the similarity between the intra cluster pixels and minimize the similarity between the pixels of different regions. The region based entropy is defined in Eq. (21).

$$H(R_j) = -\sum_{m \in V_j} \frac{L_j(m)}{S_j} \log \frac{L_j(m)}{S_j} \quad (21)$$

where R_j denotes the region of the image which makes up the j th cluster. $L_j(m)$ denotes the number of pixel in the region R_j which have gray level values of 'm'. V_j is the set of all pixel intensities that are present in the region R_j . $S_j = |R_j|$ denotes the cardinality, or the number of pixels in the R_j region. The segmented image's region entropy is given by

$$H_r(I) = \sum_{j=1}^c \left(\frac{S_j}{S_I} \right) H(R_j) \quad (22)$$

The entropy for the layout is defined as:

$$H_l(I) = -\sum_{j=1}^c \left(\frac{S_j}{S_I} \right) \log \left(\frac{S_j}{S_I} \right) \quad (23)$$

The combination of the above two entropies leads to the formation of the final entropy-based objective function in Eq.(24)

$$E = H_l(I) + H_r(I) \quad (24)$$

The lower the value of E , the better is the clustering scheme. Table II shows minimum E with respect to three test images with different noise types and for all competing algorithms. The Salt & Pepper noise added Cameraman image has been taken to represent a standard Salt & Pepper noise added image while the noisy images of the Zebra and the Mushroom represent Gaussian noise added and Poisson noise added images respectively. The lower the value of E , the better is the clustering of pixels. Our algorithm achieves lowest values of E which indicates optimal immunity to noise and outliers.

C. Increasing The Number Of Clusters

Increasing the number of clusters exposes intricate details of the test image. Fig. 7(a) shows a Salt & Pepper noise added test image while figs. 7(b) and 7(c) present the segmented images with cluster numbers 3 and 5 respectively. As can be seen from fig. 7(c), the staircase and the door nearest to it are properly visible which were not present in the 3-level segmented image.

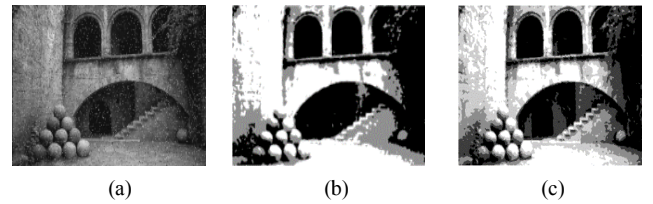


Fig. 7: a) Original Image b) 3-level c) 5-level segmentation

D. Extension To Colour Images

All colour images can be visualized as combinations of their Red, Green and Blue component images. The individual R, G, B components of the noisy colour image were separately segmented and concatenation of these separately segmented images yield the final segmented colour image, shown in Fig. 8(b), where Fig. 8(a) shows the noisy colour image.



Fig. 8: a) Noisy colour image b) Segmented image

Table I. Segmentation Accuracy (SA%) for all test images for all competing algorithms

Noise	Image	NN Cut	FLICM	RFLICM	WFLICM	KWFLICM	Proposed method
20% Salt & Pepper	Cameraman	96.4229	99.5502	99.6610	99.6984	99.7119	99.9080
30% Salt & Pepper		94.0326	99.4221	99.6059	99.6240	99.7080	99.8252
20%Gaussian		92.7009	99.0229	99.2820	99.6815	99.7015	99.8995
30%Gaussian		89.0326	98.7221	98.8059	99.1240	99.5080	99.7015
Poisson		95.0326	97.6651	98.8559	99.5420	99.7080	99.7567
20% Salt & Pepper	Zebra	95.2212	99.2142	99.4620	99.5741	99.6994	99.7180
30% Salt & Pepper		92.0326	99.1992	99.4059	99.6240	99.6221	99.6787
20%Gaussian		91.8884	99.4887	99.5779	99.6848	99.7116	99.7992
30%Gaussian		87.3312	99.4567	99.5112	99.6696	99.7002	99.7676
Poisson		92.2124	98.6651	98.8559	99.5420	99.7080	99.7567
20% Salt & Pepper	Mushroom	95.4229	99.4422	99.5757	99.6232	99.7221	99.9220
30% Salt & Pepper		93.0326	99.3121	99.4332	99.5940	99.7090	99.8796
20%Gaussian		91.7009	99.1228	99.2976	99.6731	99.6991	99.8995
30%Gaussian		88.0326	98.9222	99.1115	99.5240	99.4221	99.7598
Poisson		94.0326	98.1114	98.7665	99.4420	99.6990	99.7212

Table II. Entropy measure for all test images for all competing algorithms

Image with noise	Metric	NN Cut	FLICM	RFLICM	WFLICM	KWFLICM	Proposed method
Cameraman (30% Salt & Pepper)	$H_r(L)$	1.8124	1.7932	1.7726	1.7501	1.7291	1.7013
	$H_i(L)$	0.4684	0.4894	0.4832	0.4821	0.4795	0.4758
	E	2.2808	2.2826	2.2558	2.2322	2.2086	2.1771
Zebra (30% Gaussian)	$H_r(L)$	1.6394	1.4504	1.4548	1.4448	1.4404	1.4360
	$H_i(L)$	0.3227	0.3701	0.3798	0.3704	0.3114	0.3003
	E	1.9621	1.8205	1.8346	1.8152	1.7518	1.7363
Mushroom (Poisson)	$H_r(L)$	1.5345	1.5334	1.5307	1.5316	1.5304	1.5279
	$H_i(L)$	0.4358	0.4376	0.4404	0.4451	0.4393	0.4388
	E	1.9703	1.9710	1.9711	1.9767	1.9697	1.9667

VIII. APPLICATION TO SAR AND MEDICAL IMAGES

Synthetic Aperture Radar (SAR) images are utilized to demarcate coastlines and unknown terrain besides other applications. Speckle noise manifests itself in as apparently random placement of pixels which are conspicuously bright or dark. Fig. 9(a) shows a typical speckle-noise ridden SAR image. Medical images are typically Magnetic Resonance (MR) images ridden with special Rician type of noise. Fig. 10(a) provides a heavily Rician-noise added MR image. The segmented images and for our algorithm and other competing algorithms are presented in Figs. 9(b)-(g) and 10(b)-(g) respectively. The corresponding entropy measures are tabulated in Table 3 and our proposed method achieves lowest entropy as can be seen from the values in Table III. The SAR image considered here requires only 2 levels of segmentation.

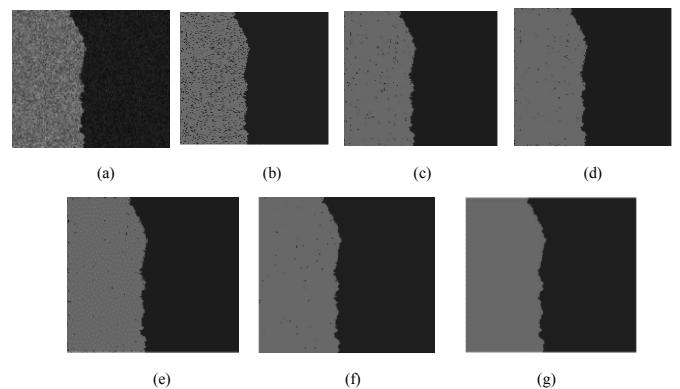


Fig. 9: a) SAR image b) NN Cut c) FLICM d) RFLICM e) WFLICM f) KWFLICM g) Proposed

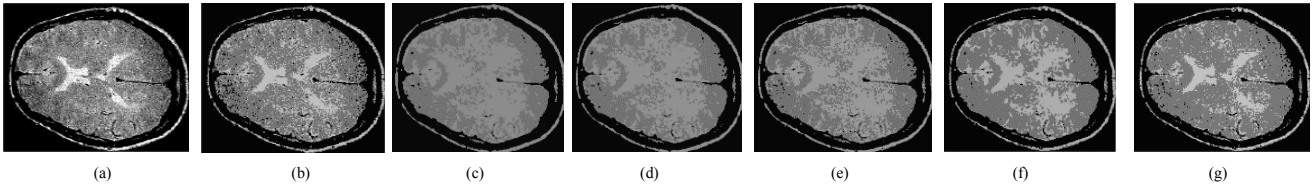


Fig. 10:a) MR image b) NNCut c) FLICM d) RFLICM e) WFLICM f) KWFLICM g) Proposed

Table III. Entropy measure for SAR and MR images

Image with noise	Metric	NN Cut	FLICM	RFLICM	WFLICM	KWFLICM	Proposed method
SAR (Speckle noise)	$H_r(L)$	0.9112	0.8923	0.8848	0.8730	0.8629	0.8596
	$H_l(L)$	0.3778	0.3953	0.3810	0.3862	0.3729	0.3669
	E	1.2890	1.2876	1.2658	1.2592	1.2358	1.2265
MR (Rician noise)	$H_r(L)$	1.6533	1.6397	1.6108	1.6065	1.5878	1.5686
	$H_l(L)$	0.3734	0.3808	0.3898	0.3867	0.3839	0.3790
	E	2.0267	2.0205	2.0006	1.9932	1.9717	1.9476

IX. A BRIEF LOOK AT THE COMPUTATIONAL TIME OF THE COMPETING ALGORITHMS

Our algorithm serves to accurately extract the accurate segmentation information from an image while removing noise and maintaining the unique structural characteristics of the image. However, when accuracy is the major bottleneck, computational complexity has to be compromised to a certain extent. The computational time was evaluated after averaging through 25 runs for 20 test images, all of sizes 481×321 , taken from the BSDS. Two of these images have been shown in the experimental section. The others could not be included for space constraint. For the results provided in Table IV, the experiments are carried out on a PC with a second generation core i5 processor running at 2.66 GHZ and having 4 GB RAM. The operating system is Windows 7 home basic and the compiler is MATLAB 7.10.0.

Table IV: Average computational time per image taken by the competing algorithms

Competing algorithms	Mean computational time in seconds
NNCUT	10.223
FLICM	512.626
RFLICM	456.242
WFLICM	412.123
KWFLICM	650.224
Proposed	330.933

As is evident from the values in the table, the NNCut algorithm requires minimum computational time since it involves spectral grouping and does not work on individual windows. However, the NNCut algorithm is not noise immune and hence does not serve the purpose of a good noisy image segmentation. Our algorithm achieves lesser computational time than the other algorithms which also incorporate spatial information into account.

X. CONCLUSION AND FUTURE WORK

The proposed algorithm shows appreciable performance for all sorts of noises. The method incorporates neighbourhood non-

homogeneity information based image segmentation involving kernel mapping. However, the parameter σ of the kernel has not been made adaptive since a variation of σ from 5 to 5000 did not reflect any appreciable change in the performance of the algorithm. We are planning on investing on other Kernel functions which would require adaptive parameter tuning, for future work.

REFERENCES:

- [1] D. L. Pham, and J. L. Prince, "An adaptive fuzzy C-means algorithm for image segmentation in the presence of intensity inhomogeneities," *Pattern Recognition Letters*, vol. 20, pp.57-68, 1999.
- [2] X. Yin, S. Chen, E. Hu, and D. Zhang, "Semi-supervised clustering with metric learning: An adaptive kernel method," *Pattern Recognit.*, vol. 43, no. 4, pp. 1320-1333, Apr. 2010.
- [3] L. Zhu, F. Chung, and S. Wang, "Generalized fuzzy C-means clustering algorithms with improved fuzzy partitions," *IEEE Trans. Syst., Man, Cybern., B*, vol. 39, no. 3, pp. 578-591, Jun. 2009.
- [4] S. Tan and N. A. M. Isa, "Color image segmentation using histogram thresholding fuzzy C-means hybrid approach," *Pattern Recognit.*, vol. 44, no. 1, pp. 1-15, 2011
- [5] Y. A. Tolias and S.M. Panas, "On applying spatial constraints in fuzzy image clustering using a fuzzy rule-based system," *IEEE Signal Processing Letters*, vol. 5, pp.245-247, 1998.
- [6] J. Dunn, "A fuzzy relative of the ISODATA process and its use in detecting compact well-separated clusters," *J. Cybern.*, vol. 3, no. 3, pp. 32-57, 1974.
- [7] J. Bezdek, *Pattern Recognition with Fuzzy Objective Function Algorithms*. New York: Plenum, 1981.
- [8] L. Szilagyi, Z. Benyo, S. Szilagyi, and H. Adam, "MR brain image segmentation using an enhanced fuzzy C-means algorithm", in *Proc. 25th Annu. Int. Conf. IEEE EMBS*, Nov. 2003, pp. 17-21.
- [9] W. Cai, S. Chen, and D. Zhang, "Fast and robust fuzzy C-means clustering algorithms incorporating local information for image segmentation," *Pattern Recognit.*, Vol. 40, No. 3, pp. 825-838, Mar. 2007.
- [10] S. Krinidis and V. Chatzis, "A robust fuzzy local information C-means clustering algorithm", *IEEE Trans. Image Process.*, vol. 19, no. 5, pp 1328-1337, May 2010.
- [11] M. Gong, Z. Zhou, and J. Ma, "Change detection in synthetic aperture radar images based on image fusion and fuzzy clustering", *IEEE Trans. Image Process.*, vol. 21, no. 4, pp. 2141-2151, Apr. 2012.
- [12] N. Cristianini and J. S. Taylor, *An Introduction to SVM's and Other Kernel-Based Learning Methods*. Cambridge, U.K.: Cambridge Univ. Press, 2000.
- [13] X. Yang and G. Zhang, "A kernel fuzzy C-means clustering-based fuzzy support vector machine algorithm for classification problems with outliers or noises", *IEEE Trans. Fuzzy Syst.*, vol. 19, no. 1, pp. 105-115, Feb. 2011.
- [14] V. Roth and V. Steinlage, "Nonlinear discriminant analysis using kernel functions", in *Advances in Neural Information Processing*

- Systems 12*, S. A. Solla, T. K. Leen, and K.-R. Muller, Eds. Cambridge, MA: MIT Press, 2000, pp. 568–574.
- [15] B. Scholkopf, A. J. Smola, and K. R. Muller, “Nonlinear component analysis as a kernel eigenvalue problem”, *Neural Comput.*, vol. 10, no. 5, pp. 1299–1319, 1998.
- [16] S. Chen and D. Zhang, “Robust image segmentation using FCM with spatial constraints based on kernel-induced distance measure”, *IEEE Trans. Sys., Man And Cybern., Part B*, Vol. 34, no. 4, pp 1907-1916, 2004.
- [17] M. Gong, Y. Liang, J. Shi, W. Ma, and J. Ma, ‘Fuzzy c-means clustering with local information and kernel metric for image segmentation”, *IEEE Trans. Image Processing* Vol.22, No 2, pp 573-584, Feb 2013
- [18] A. Lapini, T. Bianchi, F. Argenti, L. Alparone, “Blind speckle decorrelation for SAR image despeckling”, *IEEE Trans. Geosc. And Remote Sensing*, Vol. 52, Issue 2, pp 1044 - 1058, Dec. 2013.
- [19] S. Solbo and T. Eltoft, “Homomorphic wavelet-based statistical despeckling of SAR images”, *IEEE Trans. Geosc. And Remote Sensing*, Vol. 42, no. 4, pp. 711-721, April 2004.
- [20] J. C. Bezdek, L. O. Hall, and L. P. Clarke, "Review of MR image segmentation techniques using pattern recognition", *Medical Physics*, vol.20, pp.1033-1048, 1993.
- [21] D. L. Pham, C. Y. Xu, J. L. Prince, “A survey of current methods in medical image segmentation”, *Annual Review of Biomedical Engineering*, vol. 2, pp. 315 - 337, 2000.
- [22] V. Boskovitz and H. Guterman, “An adaptive neuro-fuzzy system for automatic Image segmentation and edge detection”, *IEEE Transactions on Fuzzy Systems*, Vol. 10, Issue 2, pp. 247-261, 2002.
- [23] I. Bloch, “Fuzzy sets in image processing”, *Proceedings of ACM Symposium on Applied Computing*, New York, USA, March 6-8, pp. 175 – 179, 1994.
- [24] J. C. Bezdek, R. Chandrasekhar and Y. Attikiouzel, “A geometric approach to edge detection”, *IEEE Transactions on Fuzzy Systems*, Vol. 6, Issue 1, pp. 52- 75, 1998.
- [25] C. Fowlkes, S. Belongie, F. Chung, and J. Malik, “Spectral grouping using the Nystrom method”, *IEEE Trans. Pattern Anal. Mach. Intell.*, vol. 26, no. 2, pp. 1–12, Feb. 2004.
- [26] C. Li, R. Huang, Z. Ding, J. C. Gatenby, D. N. Metaxas, and J. C. Gore, “A level set method for image segmentation in the presence of intensity in homogeneities with application to MRI”, *IEEE Trans. Image Process.*, vol. 20, no. 7, pp. 2007–2016, Jul. 2011.
- [27] H. Zhang, J. Fritts, and S. Goldman, “An entropy-based objective evaluation method for image segmentation”, *Proc. SPIE, Storage Retrieval Methods Appl. Multimedia*, vol. 5307, pp. 38–49, Jan. 2004.